Auger Recombination Suppression in Nanocrystals with Asymmetric Electron–Hole Confinement

*Juan I. Climente, Jose L. Movilla, and Josep Planelles**

Type II and quasi-type II nanocrystals with thick shells exhibit reduced blinking. However, after a number of monolayers, the influence of the shell thickness is found to vanish. Using a two-band Kane Hamiltonian, it is shown that this behavior is a consequence of interband coupling and asymmetric confinement of electrons and holes. Interface alloying provides an additional, order-of-magnitude contribution to the Auger suppression, in agreement with recent experiments. The existence is predicted of critical shell thicknesses that strongly quench Auger processes for any core size.

1. Introduction

Intermittency in the optical emission of semiconductor nanocrystals (NCs), often referred to as blinking, poses a major challenge towards development of applications in biology,[1–4] quantum optics,[5] and lasing.[6] After a decade of intense research, it is now widely believed that nonradiative Auger processes are ultimately responsible for the blinking.[7] When an electron–hole pair (exciton) is generated in the NC by absorption of light, there is a possibility that one of the two carriers becomes trapped at the surface. When the next electron–hole pair is created, it combines with the remaining carrier to form a charged exciton (trion). At this point there is a competition between radiative electron–hole recombination (emission) and nonradiative Auger recombination (AR), by which the energy of the recombining electron–hole pair is transferred to the extra carrier (**Figure 1**a). The extra carrier then moves into a highly excited (typically unbound) state and rapidly loses kinetic energy to heat. Several strategies have been used in the last few years to block some of the steps involved in this mechanism, reaching unprecedented success in the minimization of Auger processes.[7–18] One of the most impressive achievements is the complete removal of blinking in individual NCs by using a radially graded composition.[11] The graded composition translates into a smooth confining potential, which greatly suppresses AR as shown by Cragg and Efros.[19]

Another successful technique relies on the use of type-II or quasi-type-II core/shell NCs.[12–18] These structures offer a number of advantages, such as well-established and extremely precise growth techniques[20,21] and the possibility to independently engineer electron and hole wave functions. The latter enables optimization of lasing[22] and photovoltaic[23] performance, as well as control of the electron–hole exchange energy, which is required for many optoelectronic and quantum optics applications.[24] Importantly, the origin of the AR suppression in these structures has not yet been clarified. On the one hand, there is a reduction of the electron–hole overlap. Since Auger processes are of Coulomb nature this clearly contributes,[12] and yet using giant shells—where the overlap is presumably small—does not completely suppress blinking.[13,17] On the other hand, there are possible interface effects. Indeed, recent experiments in CdSe/CdS NCs suggest that electron–hole overlap alone cannot explain the observed Auger lifetimes, and interfacial alloying may provide a significant contribution.[18]

In this work, we provide theoretical assessment of the role played by each of the factors present in core/shell NCs. We consider type-I, quasi-type-II, and type-II heterostructures, and analyze how the core/shell sizes and the interface potential affect the AR rates. The results are in agreement with recent measurements and provide interpretation for the

Dr. J. I. Climente, Dr. J. L. Movilla, Prof. J. Planelles
Departament de Quimica Fisica i Analitica
Universitat Jaume I
Castelló de la Plana 12080, Spain
E-mail: josep.planelles@qfa.uji.es

DOI: 10.1002/smll.201101740

NANO MICRO small

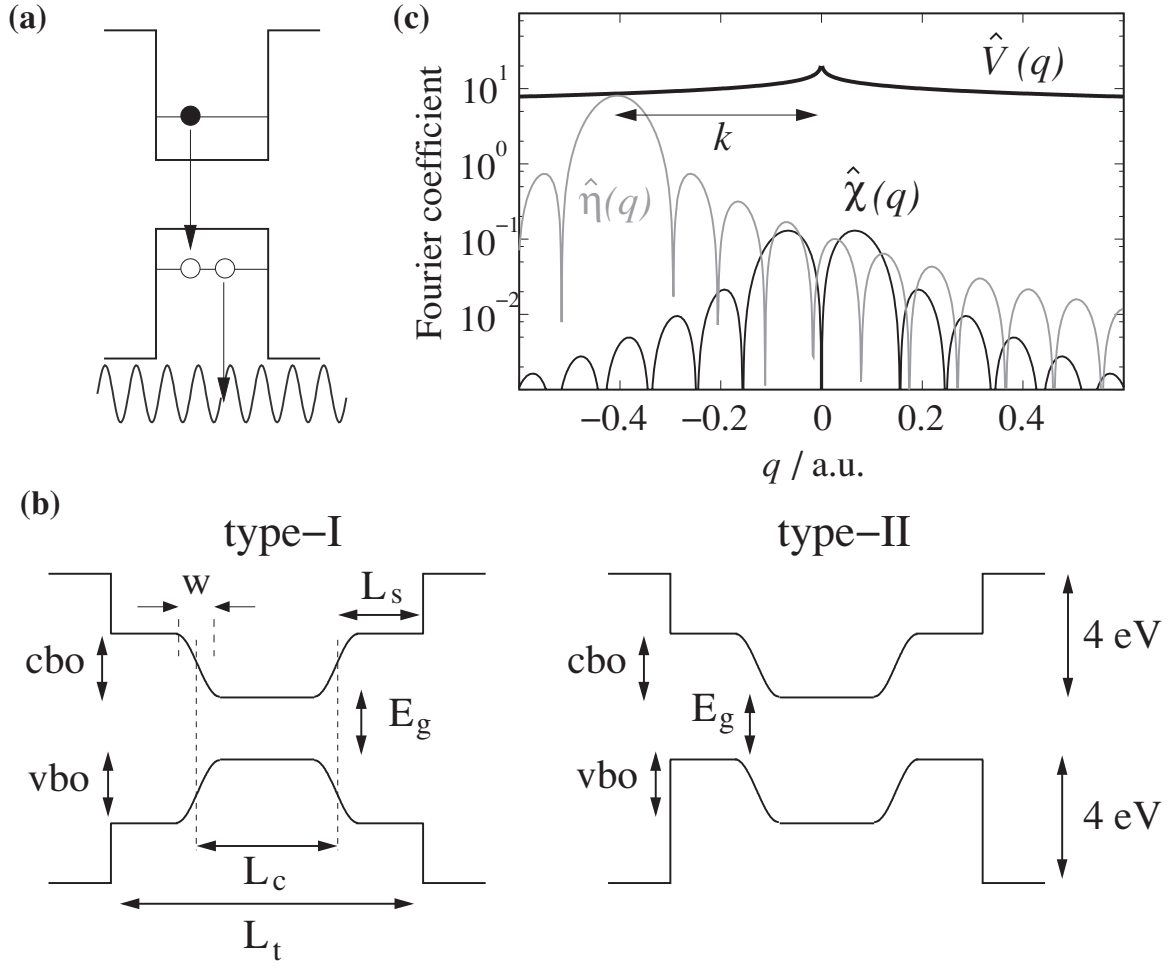

Figure 1. a) Schematic of the Auger process under study. b) Confinement potential profile used for type-I, quasi-type-II (left), and type-II NCs (right). c) Typical Fourier spectrum of the integrand terms in the Auger matrix element of Equation (5). CBO=conduction band offset, VBO=valence band offset.

experimentally observed trends. In addition, we predict the existence of a "magic" shell thickness in type-II and quasi-type-II NCs which strongly suppresses AR independently of the core size.

2. Results and Discussion

Our model is based on that which successfully explained the effect of confinement on the AR of type-I NCs.[19] Thus, we describe electrons and holes with a one-dimensional, two-band Kane Hamiltonian:[25]

$$H = \begin{pmatrix} -\frac{p^2}{2m_e} + V_c(x) + E_g/2 & Kp \\ Kp & \frac{p^2}{2m_h} - V_v(x) - E_g/2 \end{pmatrix} \quad (1)$$

where p is the momentum operator, $m_{e(h)}$ is the effective mass of the electron (hole) disregarding the influence of the valence (conduction) band, hereafter termed VB (CB). E_g is the energy gap as defined in Figure 1b, K is the Kane matrix element, and $V_{c(v)}(x)$ the CB (VB) confinement potential. The height of $V_{c(v)}(x)$ is given by the core/shell band-offset, and the shape by a cosine-like profile of width w, which accounts for compositional grading (see Figure 1b for a complete description of the potential shape). This allows us to cover all the range from abrupt interfaces ($w = 1$ Å) to alloyed interfaces spread over a few monolayers (w tens of Å). The resulting electron and hole states have a mixture of CB and VB components [Eq. (2)]:

$$\psi_i = \chi_i(x)u_c(x) + \eta_i(x)u_v(x) \quad (2)$$

with i = e,h. Here χ and η (u_c and u_v) are the envelope (periodic) parts of the Bloch wave function corresponding to the CB and VB, respectively. For electrons, the CB component χ is by far dominant. The opposite holds for holes. We consider the NC to be in the strong confinement regime. The most relevant AR process is then that illustrated in Figure 1a, where two holes and one electron are involved.[11,19,26] The AR rate is calculated using Fermi's golden rule:

$$\frac{1}{\tau_A} = \frac{2\pi}{\hbar} |\langle i| V |f\rangle|^2 \rho(E_f)\delta(E_i - E_f) \quad (3)$$

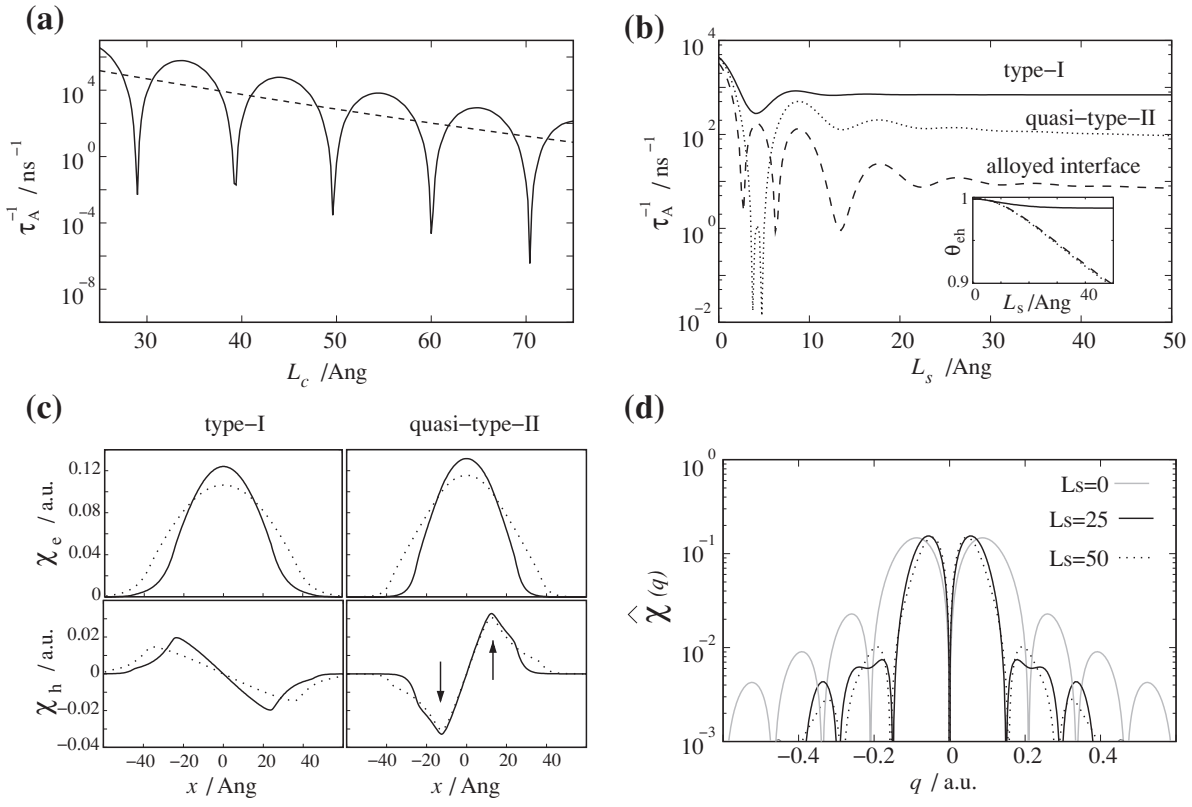

Figure 2. a) AR rate versus core size in type-I NCs (CBO = 1.5 eV, VBO = 0.5 eV, L_s = 20 Å). The dashed line is a linear fit. b) AR rate versus shell thickness. Solid/dotted/dashed lines: CBO = 1.5/0.1/0.1 eV and w = 1/1/10 Å. L_c = 25 Å. c) CB envelope function of the electron and hole ground state in atomic units (a.u.). Type-I: L_c = 25 (solid line) versus L_c = 50 Å (dotted line). Quasi-type-II: L_s = 25 (solid line) versus L_s = 50 Å (dotted line). d) Fourier spectrum of the CB term in the Auger matrix element. The inset in (b) shows the electron–hole overlap versus shell thickness.

Here, $V(r)$ is the Coulomb potential, E_i and E_f are the energies of the initial and final states, respectively, and $\rho(E_f)$ is the density of states at E_f. The initial state, $|i\rangle$, is defined by two vacancies in the lowest VB orbital (i.e., holes): $|i\rangle = \psi_h^0(x_1)\psi_h^0(x_2)\frac{1}{\sqrt{2}}\big(\alpha(1)\beta(2) - \beta(1)\alpha(2)\big)$, with α (β) standing for spin up (down) projections. In the final state, $|f\rangle$, we have promoted one vacancy to the CB and another to a highly excited VB orbital: $|f\rangle = \frac{1}{\sqrt{2}}\left(\psi_e^0(x_1)^*\psi_h^{ex}(x_2) + \psi_h^{ex}(x_1)\psi_e^0(x_2)^{*}\right)\frac{1}{\sqrt{2}}\big(\alpha(1)\beta(2) - \beta(1)\alpha(2)\big)$. The excited, unbound hole state, ψ_h^{ex}, is taken as a free electron plane wave whose momentum k is given by energy conservation. Because ψ_h^{ex} has negligible CB component, the Coulomb matrix element in Equation (3) is given by:

$$\langle i\,|V|\,f\rangle = \sqrt{2}\left(\langle\chi_h\eta_h\,|V|\,\chi_e e^{ikx_2}\rangle + \langle\eta_h\eta_h\,|V|\,\eta_e e^{ikx_2}\rangle\right) \quad (4)$$

For computational performance and physical insight, it is convenient to rewrite the above integrals in the Fourier space. For example,

$$\langle\chi_h\eta_h\,|V|\,\chi_e e^{ikx_2}\rangle = \frac{1}{2\pi}\int_{-\infty}^{\infty} dq\,\hat{V}(q)\hat{\chi}(q)\hat{\eta}(q) \quad (5)$$

where $\hat{V}(q)$ is the Fourier transform of $V(r)$, $\hat{\chi}(q) = \int dx_1\chi_h(x_1)*\chi_e(x_1)e^{iqx_1}$ is the Fourier transform of the CB components, and $\hat{\eta}(q) = \int dx_2\eta_h(x_2)*e^{i(k-q)x_2}$ that of the VB components.

AR will be fast when Equation (5) is large.[28] We can anticipate if this is the case by examining each of the integrand terms in the frequency domain. A typical case is illustrated in Figure 1c. One can see $\hat{V}(q)$ is a slowly varying function with q. Instead, $\hat{\chi}(q)$ and $\hat{\eta}(q)$ are oscillatory functions rapidly decaying away from their maxima, which are located near $q = 0$ and $q = k$, respectively. The efficiency of AR processes is thus mainly determined by the overlap between these two terms. For example, when k is small (e.g., the gap is small), the most relevant Fourier components of $\hat{\eta}(q)$ and $\hat{\chi}(q)$ are close by and AR is fast. We shall use this kind of analysis to understand the results below.

We study II–VI core/shell NCs. As a starting point, we investigated the influence of the core size in type-I NC where both electrons and holes are well confined in the core, surrounded by a shell of thickness L_s = 20 Å acting as a barrier. The core/shell interface is abrupt, w = 1 Å. The resulting AR rates are plotted in **Figure 2**a (solid line). One can see periodic valleys where AR is strongly suppressed. These "magic sizes" were first predicted by Efros and co-workers and should be detectable at low temperatures.[19,27] At room temperature, the behavior probably resembles that of the dashed line (least-squares fit). As expected from simple "volume" scaling, the bigger the core the slower the AR rate.[6,19]

NANO MICRO small

Next we explore the effect of the shell thickness and band alignment in Figure 2b. For type-I NCs we consider a high potential barrier, corresponding to, for example, CdSe/ZnS interfaces. Leaving aside the oscillatory behavior for thin shells, which will be analyzed below, the striking result is that the mere fact of adding a capping shell diminishes τ_A^{-1} by a factor of about 5, in spite of the electron and hole remaining in the core all the time. This is because the confining potential of the shell (CBO = 1.5 eV in our calculations) is lower than that of the surrounding medium (4 eV). This enables the carrier wave function to decay more slowly near the interface, thus removing high-frequency Fourier components of $\hat{\chi}(q)$ and $\hat{\eta}(q)$, which are responsible for the AR. For high barriers, this reduction is possibly too weak to influence the blinking observed experimentally.[26] However, the finding can be extended to lower barriers. We then study a quasi-type-II shell with low CBO (0.1 eV). In this case, τ_A^{-1} diminishes by two orders of magnitude. The resulting AR lifetimes are already comparable to typical radiative lifetimes (tens of nanoseconds), which explains why suppressed blinking and multiexciton emission are observed in CdSe/CdS and CdTe/CdSe NCs.[12–18] It is worth noting that the order-of-magnitude reduction is achieved in spite of the electron–hole overlap being little affected. As shown in Figure 2b (inset), the overlap, $\theta_{eh} = \langle \chi_e^0 \mid \eta_h^0 \rangle + \langle \eta_e^0 \mid \chi_h^0 \rangle$, decreases by less than 10%. This comes about because the Auger integrals are not strictly proportional to the overlap between the dominant electron–hole components, as often assumed, but rather to that between components of the same band [see Eq. (4)].

Garcia-Santamaria et al.[18] suggested that an additional contribution to the AR suppression in core/shell NCs could come from interface alloying providing a smooth confinement potential. This mechanism has been proved to be efficient in NCs with intentionally graded composition.[11,19] However, it is not clear a priori whether spontaneous, few-monolayer diffusion in standard core/shell NCs can also be efficient, especially when one of the potential barriers is very low, as is the case for quasi-type-II systems. To test this, we calculate the AR rate corresponding to a quasi-type-II NC with smooth potential spreading over w = 10 Å (2–3 monolayers). The result (dashed line in Figure 2b) confirms that even a moderate smoothing of the confining potential can provide an additional order-of-magnitude decrease of τ_A^{-1}.

Figure 2b shows that beyond L_s = 20 Å the shell thickness makes almost no difference to τ_A^{-1}, that is, there is no significant volume scaling. This is in sharp contrast to type-I NCs of varying core size (Figure 2a), and is consistent with the experiment of Mahler et al., where the thickness of the shell of CdSe/CdS NCs was found to play a limited role in the blinking statistics.[13] It is also consistent with the experiments of Garcia-Santamaria et al., where a fast decrease of τ_A^{-1} was measured for the *initial* stages of shell growth,[18] and those of Vela et al., where the percentage of nonblinking NCs seemed to reach saturation after 10–12 shell monolayers.[17] To understand this limit, in Figure 2c we compare the CB envelope functions of electron and hole ground states in a system with no saturation (type-I NCs of increasing core size) and another with saturation (quasi-type-II NCs of increasing shell size). In type-I NCs, the bigger core implies softer electron and hole wave functions (dotted lines). This removes high-frequency components in $\hat{\chi}(q)$, thus reducing the AR. In quasi-type-II NCs, the thicker shell again implies delocalizing the electron over the entire NC (see χ_e), but not the hole CB component, χ_h. As pointed out by the arrows, the wave function maxima of χ_h barely vary when enlarging the shell. This is in contrast to the type-I case and is surprising because the CB potential is nearly flat. The reason for this characteristic behavior is the interband coupling. From Equation (1), it follows that the Schrödinger equation for χ_h is [Eq. (6)]:

$$\left(-\frac{\nabla^2}{2m_e} + V_c(x) + E_g/2\right)\chi_h(x) + K\nabla\eta_h(x) = E_h^0\chi_h(x) \tag{6}$$

For the hole ground state $K\nabla\eta_h >> V_c\chi_h(x)$ and the interband term dominates over $V_c(x)$. In other words, the CB component of the hole feels the VB potential through the interband coupling.

We can now explain the asymptotic limit of Figure 2b. In the initial stages of shell growth, τ_A^{-1} experiences a decrease due to the electron (χ_e) delocalization, which removes high-frequency components in $\hat{\chi}(q)$, thus reducing Equation (5). After a certain shell thickness, the high-frequency components of $\hat{\chi}(q)$ are almost exclusively given by the hole (χ_h). Since the hole remains in the core, further extending the shell thickness provides little benefit. This is illustrated in Figure 2d, which shows $\hat{\chi}(q)$ for no shell (gray line), L_s = 25 Å (black line), and L_s = 50 Å (dotted line). While there is a clear reduction of high-frequency components from 0 to 25 Å, the reduction is small when extending to 50 Å. A similar behavior can be expected for type-II NCs as long as the confinement potential is shallow enough for interband coupling to dominate.

Let us now pay attention to the AR minima in Figure 2b. Similar minima were previously reported in type-I NCs with varying core size, as in Figure 2a, and are known to originate in destructive interferences between the electron and hole wave functions.[19,27] Figure 2b suggests that in core/shell NCs it is possible to find sharp minima by varying not only the core size but also the shell thickness. This is confirmed in **Figure 3**a, which shows a contour plot of τ_A^{-1} as a function of both core and shell thickness in quasi-type-II NCs. The remarkable result here is that a valley of strongly suppressed AR can be found for a given shell thickness regardless of the core size (L_s = 4–6 Å in Figure 3a). The same finding holds also in type-II NCs with holes localized in the shell, as in CdS/ZnSe (see Figure 3b, L_s = 8–10 and 17–19 Å), as well as in type-II and quasi-type-II structures with opposite electron and hole spatial distribution (see Supporting Information). The possibility to achieve independent control of τ_A^{-1} with either the core or the shell size is enabled by the asymmetric electron–hole confinement in these structures, and it has important practical implications for the design of NCs with negligible AR rates. On the one hand, one can take advantage of the extremely precise shell growth techniques, which allow sequential monolayer deposition, as opposed to core sizes, which are more difficult to control.[20,21] We then foresee that "magic sizes" for AR suppression will be easier to realize experimentally, eventually extending to NC ensembles with

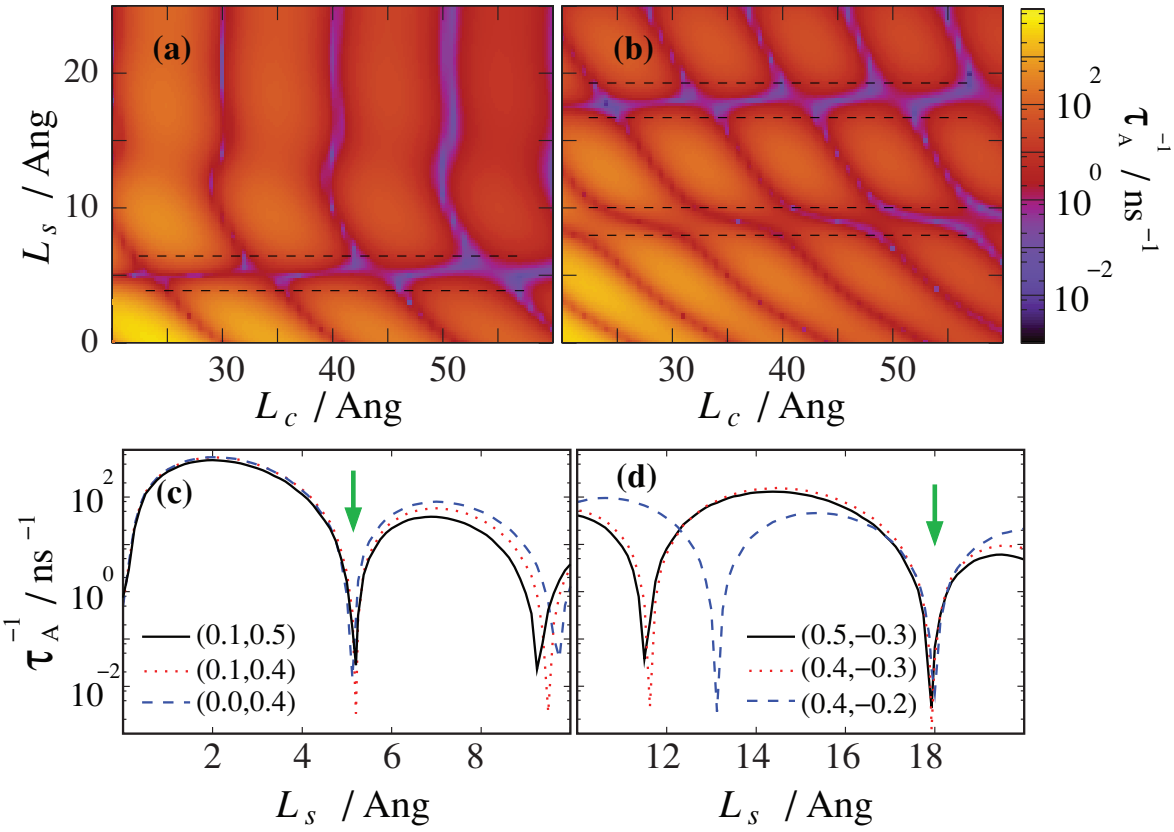

Figure 3. Top panels: contour plots of the AR rate for different core and shell sizes: a) quasi-type-II NCs, b) type-II NCs. The dashed lines highlight the regions of L_c-independent minima. Bottom panels: corresponding cross sections at L_c = 30 Å for different (CBO, VBO) values (in eV). Black lines are the case displayed in the panel above. The arrows point at the L_c-independent minima.

inhomogeneous core size distribution but identical shells. On the other hand, one may independently tune τ_A^{-1} and the exciton emission wavelength through careful core/shell design.

The observability of the AR minima in type-I NCs is hindered by random thermal and electric field fluctuations, which modify the potential seen by the carriers.[19] We investigated if the same occurs in core/shell structures with asymmetric electron–hole potential. The solid lines in Figure 3c and d show a vertical cross section of the contour plots above. One can identify a few narrow τ_A^{-1} minima with increasing L_s. The one marked with an arrow is the L_c-independent one ("magic" shell). Dotted and dashed lines represent equivalent plots but with moderate changes in the band-offset potentials. Interestingly, the potential fluctuations barely shift the position of the L_c-independent minimum. This is in contrast to the other (core-size-dependent) minima, whose position is sensitive to the fluctuations and will then be averaged out under typical experimental conditions. These results suggest that AR suppression with critical shell thicknesses may be observed even at room temperature and strong pumping power.

We close this section with a few remarks. First, we note that the predictions in Figure 3 hold if we replace the Coulomb potential by a contact interaction, $V(r) = \delta(x_1 - x_2)$ (see Supporting Information). This means that the reported phenomena do not depend on the details of the particle–particle interaction potential, and the extension to three-dimensional systems should not imply qualitative differences. Second, similar physics can be expected if the Auger process involves an excess electron instead of an excess hole, although such processes are generally slower due to the smaller density of electron states.[29] Last, we have assumed that Auger processes involve a continuum final state. In strongly confined NCs the final state may also be discrete, and then the physics is somewhat different.[19] However, we focus on II–VI NCs with large band gap and core/shell structure, which often implies moderately large size. Therefore, the final state is likely to be continuum or quasi-continuum.

3. Conclusion

We have investigated the influence of the shell on the AR processes of heterostructured NCs. We have shown that in quasi-type-II structures, increasing the shell thickness leads to reduced AR rates mainly due to the volume scaling, but a finite limit is obtained after a certain thickness due to the non-vanishing contribution of the carrier in the core. This explains the strong but incomplete suppression of blinking observed in giant shell CdSe/CdS NCs. Additional suppression can

NANO MICRO small

be ascribed to interface alloying in these structures, as suggested by recent experiments. We have also reported numerical evidence for the existence of critical shell thicknesses, which strongly quench the AR rate in NCs with asymmetric electron–hole potential. This quenching is independent of the core size and fairly robust against potential fluctuations, which points to the possibility of synthesizing NC ensembles with negligible AR rates at room temperature.

4. Theoretical Methods

Equation (1) is integrated numerically using a finite differences scheme. For the computation of τ_A^{-1}, in Equation (3) the Coulomb potential is written as $V(r) = 1/[\varepsilon(r+\delta)]$, where ε is the dielectric constant, $r = |x_1 - x_2|$, and δ is a parameter introduced to avoid the Coulomb singularity. Its Fourier transform is $\hat{V}(q) = \left(e^{-iq\delta}E_1(-iq\delta) + e^{iq\delta}E_1(iq\delta)\right)/\varepsilon$, with $E_1(x) = \int_x^\infty e^{-t}/t\,dt$ the exponential integral.[30] The excited hole state is $\psi_h^{ex} = \sqrt{\frac{1}{L}}e^{ikx}u_v$, where L is the length of the computational box. Its momentum is $k = \sqrt{2m_0\left(E_e^0 + 2E_h^0 + E_g\right)}/\hbar$, where m_0 is the free electron mass, while E_e^0 and E_h^0 are the single-particle electron and hole energies defined with respect to the CB and VB edges, respectively. The density of states $\rho(E_f)$ can be approximated by that of the hole in the continuum (computational box), $\rho(E_f) \approx \frac{L}{\hbar\pi}\sqrt{m_0/2E_h^{ex}}$, where $E_h^{ex} = \left(k^2/2m_0 - \mathrm{VBO}\right)$ is the single-particle energy of the plane wave subtracting the VBO. Note that L in $\rho(E_f)$ cancels the L factor arising from the plane wave normalization constants in $|\langle i|\,V\,|f\rangle|^2$.

For the simulations, we take material parameters close to those of typical II–VI NCs. The electron and hole effective masses are $m_e = 0.15m_0$ and $m_h = 0.6m_0$, respectively. The gap is $E_g = 1.5$ eV.

The Kane parameter is $K = (21\ \mathrm{eV}/2m_0)^{1/2}$, the dielectric constant $\varepsilon = 6$, and $\delta = 10^{-2}$ Å. A high potential barrier, 4 eV, is set at the external medium. The core/shell potential barrier has variable height and, unless otherwise stated, its shape is abrupt, $w = 1$ Å.

Supporting Information

Supporting Information is available from the Wiley Online Library or from the author.

Acknowledgements

Support from MICINN projects CTQ2008-03344 and CTQ2011-27324, UJI-Bancaixa project P1-1A2009-03, and the Ramon y Cajal program (JIC) is acknowledged.

[1] M. Bruchez, M. Moronne, P. Gin, S. Weiss, A. P. Alivisatos, *Science* **1998**, *281*, 2013.
[2] W. C. W. Chan, S. M. Nie, *Science* **1998**, *281*, 5385.
[3] M. Dahan, S. Levi, C. Luccardini, P. Rostaing, B. Riveau, A. Triller, *Science* **2003**, *302*, 442.
[4] X. Michalet, F. F. Pinaud, L. A. Bentolila, J. M. Tsay, S. Doose, J. J. Li, G. Sundaresan, A. M. Wu, S. S. Gambhir, S. Weiss, *Science* **2005**, *307*, 538.
[5] P. Michler, A. Imamoglu, M. D. Mason, P. J. Carson, G. F. Strouse, S. K. Buratto, *Nature* **2000**, *406*, 968.
[6] V. I. Klimov, A. A. Mikhailovsky, D. W. McBranch, C. A. Leatherdale, M. G. Bawendi, *Science* **2000**, *287*, 1011.
[7] A. L. Efros, *Nat. Mater.* **2008**, *7*.
[8] M. Hamada, S. Nakanishi, T. Itoh, M. Ishikawa, V. Biju, *ACS Nano* **2010**, *4*, 4445.
[9] Isnaeni, K. H. Kim, D. L. Nguyen, H. Lim, P. T. Nga, Y. H. Cho, *Appl. Phys. Lett.* **2011**, *98*, 012109.
[10] Y. Kobayashi, T. Nishimura, H. Yamaguchi, N. Tamai, *J. Phys. Chem. Lett.* **2011**, *2*, 1051.
[11] X. Wang, X. Ren, K. Kahen, M. A. Hahn, M. Rajeswaran, S. Maccagnano-Zacher, J. Silcox, G. E. Cragg, A. L. Efros, T. D. Krauss, *Nature* **2009**, *459*, 686.
[12] D. Oron, M. Kazes, U. Banin, *Phys. Rev. B* **2007**, *75*, 035330.
[13] B. Mahler, P. Spinicelli, S. Buil, X. Quelin, J. P. Hermier, B. Dubertret, *Nat. Mater.* **2008**, *7*, 659.
[14] P. Spinicelli, S. Buil, X. Quelin, B. Mahler, B. Dubertret, J. P. Hermier, *Phys. Rev. Lett.* **2009**, *102*, 136801.
[15] R. Osovsky, D. Cheskis, V. Kloper, A. Sashchiuk, M. Kroner, E. Lifshitz, *Phys. Rev. Lett.* **2009**, *102*, 197401.
[16] F. Garcia-Santamaria, Y. Chen, J. Vela, R. D. Schaller, J. A. Hollingsworth, V. I. Klimov, *Nano Lett.* **2009**, *9*, 3482.
[17] J. Vela, H. Htoon, Y. Chen, Y. S. Park, Y. Ghosh, P. M. Goodwin, J. H. Werner, N. P. Wells, J. L. Casson, J. A. Hollingsworth, *J. Biophotonics* **2010**, *3*, 706.
[18] F. Garcia-Santamaria, S. Brovelli, R. Viswanatha, J. A. Hollingsworth, H. Htoon, S. A. Crooker, V. I. Klimov, *Nano Lett.* **2011**, *11*, 687.
[19] G. E. Cragg, A. L. Efros, *Nano Lett.* **2010**, *10*, 313.
[20] J. J. Li, A. Wang, W. Guo, J. C. Keay, T. D. Mishima, M. B. Johnson, X. Peng, *J. Am. Chem. Soc.* **2003**, *125*, 12567.
[21] R. Xie, U. Kolb, J. Li, T. Basche, A. Mews, *J. Am. Chem. Soc.* **2005**, *127*, 7480.
[22] V. I. Klimov, S. A. Ivanov, J. Nanda, M. Achermann, I. Bezel, J. A. McGuire, A. Piryatinski, *Nature* **2007**, *447*, 441.
[23] H. Zhu, N. Song, T. Lian, *J. Am. Chem. Soc.* **2011**, *133*, 8762.
[24] S. Brovelli, R. D. Schaller, S. A. Crooker, F. Garcia-Santamaria, Y. Chen, R. Viswanatha, J. A. Hollingsworth, H. Htoon, V. I. Klimov, *Nat. Commun.* **2011**, *2*, 280.
[25] B. A. Foreman, *Phys. Rev. B* **1997**, *56*, R12748.
[26] C. D. Heyes, A. Yu. Kobitski, V. V. Breus, G. U. Nienhaus, *Phys. Rev. B* **2007**, *75*, 125431.
[27] D. I. Chepic, A. L. Efros, A. I. Ekimov, M. G. Ivanov, V. A. Kharchenko, I. A. Kudriavtsev, T. V. Yazeva, *J. Lumin.* **1990**, *47*, 113.
[28] The same applies to $\langle \eta_h \eta_h\,|V|\,\eta_e e^{ikx_2}\rangle$. Because the behavior is analogous, in the analysis we will only discuss $\langle \chi_h \eta_h\,|V|\,\chi_e e^{ikx_2}\rangle$
[29] J. I. Climente, J. L. Movilla, J. Planelles, arxiv:1111.1526v1.
[30] M. Abramowitz, I. A. Stegun, *Handbook of Mathematical Functions*, Dover Publications, New York, **1972**.

Received: August 24, 2011
Published online: January 5, 2012

